UNIVERSITÀ
DEGLI STUDI
DI PADOVA

UNIVERSITÀ DEGLI STUDI DI PADOVA

Dipartimento di Fisica e Astronomia "Galileo Galilei"

Corso di Laurea Triennale in Fisica

Tesi di Laurea

Individuazione di sistemi a due livelli in modelli di Tantala amorfa

Search for two-level systems in models of amorphous Tantala

Relatore

Prof. Paolo Umari

Laureando

Alessandro Corso

Anno Accademico 2023/2024

Riassunto

Lo studio della dissipazione meccanica nei vetri è fondamentale per la riduzione del rumore in apparati ottici che richiedono un'elevatissima precisione, come gli interferometri per la rilevazione di onde gravitazionali. In questi esperimenti, infatti, la maggiore limitazione alla sensibilità dello strumento risulta essere l'agitazione termica nei rivestimenti a specchio delle masse di test, rivestimenti nei quali sono impiegati materiali amorfi come la tantala (Ta_2O_5 amorfa).

Il rumore termico è causato da fluttuazioni microscopiche nella configurazione del materiale: dal teorema fluttuazione-dissipazione, una misura della potenza spettrale del rumore si ottiene dal fattore di perdita per la dissipazione meccanica. Per modellizzare tali movimenti microscopici e calcolarne la dissipazione, è stato proposto più di quattro decenni fa un semplice modello teorico basato su una doppia buca di potenziale, la quale definisce un sistema a due livelli. L'origine microscopica di tali sistemi nel materiale, tuttavia, non è ancora chiara e una sua migliore comprensione è indispensabile per indirizzare la ricerca di materiali che minimizzino il rumore.

In questa tesi, dopo aver esposto il modello e le sue predizioni per la dissipazione meccanica, si analizzano i risultati della ricerca di sistemi a due livelli effettuata in modelli realistici di Ta_2O_5 amorfa. I campioni vengono creati usando potenziali interatomici classici e viene poi usato il metodo di attivazione e rilassamento (ARTn) per trovare coppie di configurazioni strutturali vicine e la corrispondente barriera di potenziale: queste sono realizzazioni fisiche dei proposti sistemi a due livelli. Infine, vengono analizzate le caratteristiche microscopiche dei sistemi trovati e le quantità richieste per poter calcolare a partire da questi il fattore di qualità per la dissipazione meccanica.

I risultati ottenuti riproducono qualitativamente le curve sperimentali, dimostrando l'utilità delle simulazioni numeriche nella ricerca dei materiali da utilizzare nella prossima generazione di interferometri gravitazionali. I valori del fattore di qualità a temperatura ambiente sono, inoltre, in ragionevole accordo quantitativo con i risultati sperimentali ottenuti su campioni dello stesso materiale. Questo accordo mette in evidenza come ARTn, l'algoritmo di ricerca utilizzato, sia una promettente alternativa ai metodi basati sulla dinamica, in particolare per la ricerca dei sistemi a due livelli con alta barriera di attivazione, che sono fondamentali per la dissipazione a temperatura ambiente.

Grazie alla caratterizzazione microscopica dei sistemi trovati vengono poi messe in evidenza le proprietà dei sistemi maggiormente responsabili della dissipazione maccanica nell'intervallo di temperature e frequenze considerato. In particolare, si osserva che la maggior parte di questi sistemi più dissipativi sembra essere riconducibile a un preciso movimento microscopico, osservato in precedenza anche in modelli di SiO_2 amorfo. Si evidenziano, infine, le potenzialità e le criticità dell'approccio utilizzato, applicato qui per la prima volta alla tantala.

Contents

Introduction

Computing the mechanical dissipation of a glass is a problem of interest in recent material science research, and finds an important application in studying how to reduce noise in gravitational waves interferometers [6]. For these experiments the most important source of noise are thermal fluctuation arising in the mirror coatings of the test masses: these coatings are made of multiple strata of a low-refractive material (amorphous SiO_2) alternated with a high-refractive one (TiO_2 doped amorphous Ta_2O_5), the latter being the source of most noise. This is the main reason behind the efforts into understanding the origin of mechanical dissipation in a-Ta_2O_5, also called tantala, at temperatures ranging from room-temperature to cryogenic and for frequencies between 10 Hz and 10 kHz, where the interferometers are most sensitive. This knowledge can then be used to select materials and experimental conditions to minimize noise.

Thermal noise arises from mechanical dissipation due to structural relaxations. A possible model for these movements is the so called two-level systems model (TLS), which was proposed almost 50 year ago and has been succesful in explaining both thermal and acoustic properties of amorphous materials [7][3]. The model, however, does not provide any insight on the physical origin of these two-level systems and cannot predict their properties and density. The speed reached in molecular dynamics simulations has opened the possibility of observing these microscopical movements in accurate models of amorphous materials. This has been done for both SiO_2 [2] and Ta_2O_5 [14], but this approach is computationally expensive: the characteristic time of a movement relevant to dissipation is of the order of the inverse of the frequency of the dissipated excitation, and for our range of frequencies these times are astronomically large with respect to microscopical timescales. This drawback has led Barkema and Mousseau to develop a method that does not require to wait for the system to move between two configurations but actively searches for possible reaction paths in the configurational energy landscape [1]. This method, called activation-relaxation technique (ART), was recently applied to TLS search in amorphous silicon [10].

In this thesis work we have applied the ART method to amorphous tantala in order to study its mechanical dissipation, measured as a function of temperature and frequency by the loss angle Q^{-1}. In chapter 1 we review the TLS model, focusing on the derivation of the loss angle of the material, while in chapter 2 we present our results for the distribution and properties of TLSs in tantala and ultimately for the loss angle, obtained applying the TLS model to the TLSs found.

Chapter 1

Theory of dissipation in glasses

1.1 Two level systems

The two-level system (TLS) model is based on the claim that the local configuration of a glass can occasionally jump between two equilibrium configurations, close but separated by a potential barrier. Let x be the reaction coordinate of the process: we assume that the movement between the two local minima can be modelled as the motion of a particle of some mass m on the one dimensional line under a bistable potential $V(x)$. The details of the potential, as we will see, are not important: the result depends only on a few parameters, shown in figure 1.1. Note that the mass m and the x coordinate do not refer to a specific particle but should be interpreted as suitable collective parameters that describe the movement. The precise microscopical meaning of these is unknown and linked to the microscopical origin of these movements, which we will discuss in the second chapter.

The jump between the two configurations is made possible by two different mechanisms: thermal agitation and quantum tunneling. Thermally activated transitions are possible because the system is part of a much bigger environment it can exchange energy and momentum with. Tunneling lets the system move across a barrier thanks to the coherent superposition of the ground states of the two minima. For a given TLS, at low temperatures we expect the thermally activated process to be negligible and tunneling to be dominant; as the temperature rises, the coupling with the external bath favors more frequent thermal jumps but tunneling becomes impossible due to the loss of coherence. Conversely, at a fixed finite temperature, we will see that only TLS of a relatively high barrier contribute significantly to dissipation via the thermal process, while tunneling is possible only in TLS with relatively low barrier and small distance between the two minima.

In the section 1.2 we present a simple derivation of the loss angle term due to thermally activated processes only, which we will call relaxation term. This derivation does not consider the quantum mechanical nature of the system and therefore cannot account for coherent processes. In the following section 1.3 we will then see how to derive a generalisation of this result valid also in the low temperature regime where quantum processes are significant. We will obtain two terms: the first is the relaxation term, and reduces to the previous result in the classical limit; the second, which we will call resonance term, is of purely quantum mechanical nature.

Figure 1.1: The bistable potential $V(x)$ of a two-level system

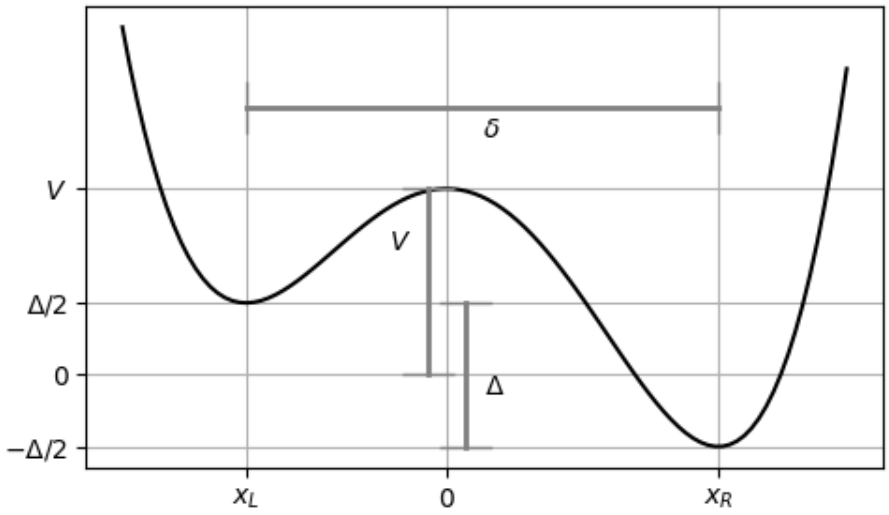

1.2 A simple model for elastic relaxation

1.2.1 Unperturbed Master equation

Let $X(t)$ be the stochastic process describing the position of the particle at time t. In this model we think of the particle as a mesoscopic particle of mass m moving on the line under a potential $V(x)$, immersed in a bath at temperature T. The particle is subject to Brownian motion: if $X(0) = x_L$ is the initial position, it will stay for a time in the left well, until it receives a strong enough thermal push to overcome the barrier, after which it will very quickly relax close to x_R, and start the process again. We call escape time the mean time the particle takes to jump across the barrier.

In the high friction limit one can derive that the mean first passage time over a high barrier U is given by Kramer's expression:

$$\tau = \tau_0 e^{\beta U}$$

where τ_0 is the inverse attempt rate, a parameter that in principle depends on geometric factors (the second derivatives of the potential at the minimum, i.e. its characteristic frequency, and at the saddle point). A derivation of this classical result is shown in appendix A.

For our specific case (figure 1.1), the escape times from the left and right well are respectively

$$\begin{aligned} \tau_{12} &= \tau_0 e^{\beta(V+\frac{\Delta}{2})} \\ \tau_{12} &= \tau_0 e^{\beta(V-\frac{\Delta}{2})} \end{aligned} \tag{1.1}$$

where we have assumed for simplicity that the two wells have the same characteristic frequency.

Since under our assumptions the particle spends most of the time in each well very close to its center, we can coarsely describe the particle as having two possible states, 1 and 2, and some transition probability between the two. Let us call $p(t)$ the probability of finding the particle in state 1 at time t. Its variation $dp(t)$ in time dt has two contributions given by particles escaped in this time from 1 and 2: $dp(t) = -p(t)/\tau_{12}dt + (1 - p(t))/\tau_{21}dt$. In the absence of any perturbation the process then

evolves towards equilibrium following

$$\dot{p}(t) = -\frac{p(t)}{\tau_{12}} + \frac{1-p(t)}{\tau_{21}} = -\frac{\tau_{12}+\tau_{21}}{\tau_{12}\tau_{21}}p(t) + \frac{1}{\tau_{21}} =: -\frac{1}{\tau}(p(t) - p_{eq})$$

where $p_{eq} \coloneqq \frac{\tau_{12}}{\tau_{12}+\tau_{21}} = \frac{1}{2}(1 + \tanh(\frac{\beta}{2}\Delta))$ is the equilibrium or asymptotical probability and

$$\tau \coloneqq \frac{\tau_{12}\tau_{21}}{\tau_{12}+\tau_{21}} = \frac{\tau_0 e^{\beta V}}{e^{\frac{\beta}{2}\Delta} + e^{-\frac{\beta}{2}\Delta}} = \frac{\tau_0}{2}e^{\beta V}\operatorname{sech}\Big(\frac{\beta}{2}\Delta\Big)$$

is the relaxation time of the TLS. By defining $q(t) = p(t) - p_{eq}$ we simply have

$$\dot{q}(t) = -\frac{1}{\tau}q(t) \tag{1.2}$$

In the absence of a perturbation, the solution for $q(t)$ is a simple decaying exponential with characteristic time τ.

1.2.2 Interaction with a phonon

We now want to consider the dynamics of the TLS when perturbed by the passage of an acoustic perturbation: a periodic deformation of the surroundings of the system. Let $V_e(x,t)$ be the perturbation of the potential caused by the deformation: $V_e(x,t)$ is a wave, propagating let's say in the positive x direction. Since we are interested in small perturbations and will consider the first order linear response of the system, we can simply choose $V_e(x,t)$ to be a plane wave of pulse ω and wave-number k: a generic perturbation can be obtained by superimposing plane waves. We also assume that the wavelength of the perturbation is much greater than the size of the system δ: typical two-level systems involve less then 100 atoms, located within a distance of order 10 Å, which is much shorter that the wavelength of mechanical waves of the considered frequencies (between 10 Hz and 10kHz). In this dipole approximation the perturbation is

$$V_e(x,t) = V_e(\omega t - kx) \approx V_e(\omega t) - V_e'(\omega t)kx + \frac{1}{2}V_e''(\omega t)(kx)^2 + \mathcal{O}((kx)^3)$$

Since the 0^{th} order is constant and physically irrelevant, the leading physical term is the first-order term. Discarding higher-order terms, the perturbation is spatially anti-symmetric: its effect is a periodic modification of the asymmetry Δ which leaves the barrier height V constant. Let

$$\tilde{\Delta}(t) = \Delta + 2\gamma e(t)$$

be the first order corrected asymmetry, where $e \ll 1$ is the strain of the system and γ is the deformation potential: $\gamma = \frac{1}{2}\frac{\partial\Delta}{\partial e}$

Assuming that the frequency of the perturbation is much lower that the attempt rate τ_0^{-1} the system

still evolves according to 1.2 but with instantaneous time-dependent escape times

$$\tilde{\tau_{12}}(t) = \tau_0 e^{\frac{V}{k_B T}} e^{\frac{\beta}{2}\tilde{\Delta}(t)} = \tau_{12} e^{\beta\gamma e(t)}$$
$$\tilde{\tau_{21}}(t) = \tau_0 e^{\frac{V}{k_B T}} e^{-\frac{\beta}{2}\tilde{\Delta}(t)} = \tau_{21} e^{-\beta\gamma e(t)}$$

For $e \ll 1$:

$$\tilde{p}_{eq}(t) = \frac{1}{2}\Big(1 + \tanh\Big(\frac{\beta}{2}(\Delta + 2\gamma e)\Big)\Big) \approx \frac{1}{2}\Big(1 + \tanh\Big(\frac{\beta}{2}\Delta\Big)\Big) + \frac{\beta\gamma}{2}\mathrm{sech}^2\Big(\frac{\beta}{2}\Delta\Big)e =: p_{eq} + q_D e$$
$$\tilde{\tau}(t) = \frac{\tau_0}{2} e^{\beta V}\mathrm{sech}\Big(\frac{\beta}{2}(\Delta + 2\gamma e)\Big) \approx \tau\Big(1 + \beta\gamma\,\mathrm{cotanh}\Big(\frac{\beta}{2}\Delta\Big)e\Big)$$

Substituting into 1.2 and keeping only first order terms in e (and observing that asymptotically q is also of order e):

$$\dot{q}(t) = -\frac{1}{\tilde{\tau}(t)}(p(t) - \tilde{p}_{eq}(t)) = -\frac{1}{\tau}\frac{q(t) - q_D e(t) + \mathcal{O}(e^2)}{1 + \mathcal{O}(e)} \approx -\frac{q(t)}{\tau} + \frac{q_D}{\tau}e(t) \tag{1.3}$$

With $e(t) = e_0 e^{i\omega t}$ an asymptotic solution to 1.3 is

$$q(t) = \chi(\omega)e(t) = \frac{q_D}{1 + i\omega\tau}e(t)$$

a compact expression of the linear response of the system. Introducing an analogy with the theory of magnetisation which will become clearer in the following section, χ is called the (transverse) dynamical susceptibility of the system.

1.2.3 Loss angle

We now compute the contribution $\delta\mathcal{E}$ of the single TLS to the complex elastic modulus $\mathcal{E}$, defined as the ratio between stress σ and strain e. The TLS's contribution to the internal energy is

$$\delta U(T, p, e) = p\Big(\frac{\Delta}{2} + \gamma e\Big) + (1 - p)\Big(-\frac{\Delta}{2} - \gamma e\Big) = (\Delta + 2\gamma e)\Big(p - \frac{1}{2}\Big)$$

The stress is defined as $\sigma = \frac{\partial u}{\partial e}$ where u is the energy density. Using a reciprocity relation analogous to a Maxwell's relation in thermodynamics we can obtain the single TLS's contribution to the stress and to the elastic modulus:

$$\frac{\partial(\delta\sigma)}{\partial p} = \frac{\partial}{\partial p}\frac{\partial(\delta U)}{\partial e} = 2\gamma \implies \delta\sigma = 2\gamma\delta p = 2\gamma q = 2\gamma\chi e$$
$$\delta\mathcal{E} = \frac{\delta\sigma}{e} = \frac{1}{e}(2\gamma\chi e) = 2\gamma\chi$$

Finally then the system's contribution to the loss angle Q^{-1} is

$$\delta Q^{-1} = \frac{Im(\delta\mathcal{E})}{Re(\mathcal{E})} = \frac{2\gamma}{Y}Im(\chi) = \frac{\gamma^2}{k_B T Y}\frac{\omega\tau}{1 + (\omega\tau)^2}\mathrm{sech}^2\Big(\frac{\Delta}{2k_B T}\Big) \tag{1.4}$$

A few remarks on this result, which we will use in chapter 2:

- At a fixed temperature, $\delta Q^{-1}(\omega)$ shows a resonance curve peaked at $\omega\tau = 1$: dissipation is

highest when the inverse pulse of the phonon is equal to the relaxation time of the TLS;

- the relaxation time itself depends on the barrier height and the temperature, being much higher at lower temperatures or for higher barriers: $\tau = 2\tau_0 e^{\beta V}\operatorname{sech}\left(\frac{\beta}{2}\Delta\right)$;
- the magnitude of δQ^{-1} decreases rapidly for increasing asymmetry Δ.

Now suppose we have a sample of volume Ω and N two-level systems: given the parameters of each of these we might compute the total loss angle at a given temperature T and pulse ω

$$Q^{-1}(\omega, T) = \frac{1}{\Omega}\sum_{i=1}^{N}\delta Q_i^{-1} = \frac{n}{k_B T Y}\frac{1}{N}\sum_{i=1}^{N}\frac{\gamma_i^2\omega\tau_i}{1+(\omega\tau_i)^2}\operatorname{sech}^2\Big(\frac{\Delta_i}{2k_BT}\Big) \tag{1.5}$$

where n is just the number of TLS per unit volume.

The former expression will be useful in chapter 2 and is the exact computation for a specific finite sample of material. For theoretical purposes it is more meaningful to compute the expected loss angle: let $n(V, \Delta, \gamma, \tau_0)$ be the distribution of TLS as a function of the relevant parameters, normalised to n:

$$\int n(V, \Delta, \gamma, \tau_0)\, dV d\Delta d\gamma d\tau_0 = n$$

Then the expected total loss angle is

$$Q(\omega, T)^{-1} = \frac{1}{k_B T Y}\int \frac{\gamma^2\omega\tau(V,\Delta,\tau_0)}{1+(\omega\tau(V,\Delta,\tau_0))^2}\operatorname{sech}^2\Big(\frac{\Delta}{2k_BT}\Big)n(V, \Delta, \gamma, \tau_0)\, dV d\Delta d\gamma d\tau_0$$

Note that often in literature it is assumed that γ and τ_0 can effectively be taken as constants. Than the summation reduces only over Δ and V

$$Q(\omega, T)^{-1} = \frac{1}{k_B T Y}\int \frac{\gamma^2\omega\tau(V,\Delta)}{1+(\omega\tau(V,\Delta))^2}\operatorname{sech}^2\Big(\frac{\Delta}{2k_BT}\Big)n(V, \Delta)\, dV d\Delta$$

and with further hypotheses on $n(V, \Delta)$ the explicit calculation can be performed and compared with experimental data [3].

1.3 The tunneling model: relaxation and resonance

The simple classical model outlined in section 1.2 is not applicable at very low temperatures, where tunneling is important. In this section we review the quantum mechanical model of a two-level-system, following steps very similar to those taken in section 1.2 with the classical model.

1.3.1 Unperturbed hamiltonian of the two-level system

Let H_0 be the hamiltonian operator of a particle of mass m moving in the one-dimensional line under the potential $V(x)$, a bistable potential as the one in figure 1.1. Without loss of generality we assume the saddle point to be located at the origin. Let $V_L(x)$ and $V_R(x)$ be the harmonic potentials approximating $V(x)$ near the center of the left and right well. For simplicity we assume, as was done in section 1.2, that the two wells have the same characteristic frequency ω_w. Let then $|\Psi_L\rangle$ and $|\Psi_R\rangle$ be the eigenvectors of the ground states of $V_L(x)$ and $V_R(x)$, and H_L and H_R the

hamiltonian operators of the two harmonic wells:

$$H_L \left|\Psi_L\right\rangle = \frac{\Delta}{2} \left|\Psi_L\right\rangle$$
$$H_R \left|\Psi_R\right\rangle = -\frac{\Delta}{2} \left|\Psi_R\right\rangle$$

translating the potential by $\frac{\hbar\omega_w}{2}$ for simplicity.

We assume that $\hbar\omega_w \gg \Delta$ and the system is very close to equilibrium: this is an analogous request to the high friction limit considered in section 1.2. Then the excited states of both wells are practically not accessible. In this limit a generic state of the system is a linear combination of the two ground states. This is why we refer to this model as a two-level system: only the two states of lowest energy are allowed.

Since $|\Psi_L\rangle$ and $|\Psi_R\rangle$ are not orthogonal we use their symmetric and antisymmetric combinations

$$|\Psi_+\rangle = \frac{|\Psi_L\rangle + |\Psi_R\rangle}{\| \, |\Psi_L\rangle + |\Psi_R\rangle \|} = \frac{|\Psi_L\rangle + |\Psi_R\rangle}{\sqrt{2}\sqrt{1+S}} = \frac{|\Psi_L\rangle + |\Psi_R\rangle}{\sqrt{2}} + \mathcal{O}(S)$$
$$|\Psi_-\rangle = \frac{|\Psi_L\rangle - |\Psi_R\rangle}{\| \, |\Psi_L\rangle - |\Psi_R\rangle \|} = \frac{|\Psi_L\rangle - |\Psi_R\rangle}{\sqrt{2}\sqrt{1-S}} = \frac{|\Psi_L\rangle - |\Psi_R\rangle}{\sqrt{2}} + \mathcal{O}(S)$$
$$\text{where } S \coloneqq \langle\Psi_L|\Psi_R\rangle \approx e^{-\frac{\delta^2}{4x_w^2}} \ll 1 \text{ and } x_w = \sqrt{\hbar/(m\omega_w)}$$

as an orthonormal basis of the two dimensional space considered. We assume the overlap S of the two ground states to be very small, note however that $|\Psi_+\rangle$ and $|\Psi_-\rangle$ are exactly orthonormal.

To find the matrix representation of the unperturbed hamiltonian operator H_0 we first need to compute the following, using $H_0 = H_L + V - V_L = H_R + V - V_R$:

$$\langle\Psi_L|H_0|\Psi_L\rangle = \langle\Psi_L|H_L + (V - V_L)|\Psi_L\rangle = \frac{\Delta}{2} + \langle\Psi_L|V - V_L|\Psi_L\rangle =: \frac{\Delta}{2} + A_L$$
$$\langle\Psi_R|H_0|\Psi_R\rangle = \langle\Psi_R|H_R + (V - V_R)|\Psi_R\rangle = -\frac{\Delta}{2} + \langle\Psi_R|V - V_R|\Psi_R\rangle =: -\frac{\Delta}{2} + A_R$$
$$\langle\Psi_L|H_0|\Psi_R\rangle = \langle\Psi_L|H_R + (V - V_R)|\Psi_R\rangle = -S\frac{\Delta}{2} + \langle\Psi_L|V - V_R|\Psi_R\rangle =: -S\frac{\Delta}{2} + S\delta V_R$$
$$\langle\Psi_R|H_0|\Psi_L\rangle = \langle\Psi_R|H_L + (V - V_L)|\Psi_L\rangle = S\frac{\Delta}{2} + \langle\Psi_R|V - V_L|\Psi_L\rangle =: S\frac{\Delta}{2} + S\delta V_L$$

Then we have

$$\begin{aligned}\langle\Psi_+|H_0|\Psi_+\rangle &= \frac{1}{2(1+S)}(\langle\Psi_L|H_0|\Psi_L\rangle + \langle\Psi_R|H_0|\Psi_R\rangle + \langle\Psi_L|H_0|\Psi_R\rangle + \langle\Psi_R|H_0|\Psi_L\rangle) \\ &= \frac{1}{1+S}(\frac{A_L + A_R}{2} + S\frac{\delta V_L + \delta V_R}{2}) =: \frac{1}{1+S}(\overline{A} + S\overline{\delta V})\end{aligned}$$
$$\langle\Psi_-|H_0|\Psi_-\rangle = \frac{1}{1-S}(\overline{A} - S\overline{\delta V})$$
$$\langle\Psi_+|H_0|\Psi_-\rangle = \frac{\Delta(1+S)}{2\sqrt{1-S^2}}$$
$$\langle\Psi_-|H_0|\Psi_+\rangle = \frac{\Delta(1-S)}{2\sqrt{1-S^2}}$$

so finally, only keeping the leading order in S

$$H_0 = \begin{pmatrix} \langle\Psi_+|H_0|\Psi_+\rangle & \langle\Psi_-|H_0|\Psi_+\rangle \\ \langle\Psi_+|H_0|\Psi_-\rangle & \langle\Psi_-|H_0|\Psi_-\rangle \end{pmatrix} \approx \overline{A}\mathbb{I} + \frac{1}{2}\begin{pmatrix} \Delta_0 & \Delta \\ \Delta & -\Delta_0 \end{pmatrix}, \ \Delta_0 \coloneqq 2S\overline{\delta V}$$

and translating the potential by $\overline{A}$

$$H_0 = \frac{1}{2}\begin{pmatrix} \Delta_0 & \Delta \\ \Delta & -\Delta_0 \end{pmatrix}$$

Defining $\tan(2\theta) = \frac{\Delta}{\Delta_0}$ the eigenstates and eigenvalues of H_0 are

$$|\Psi_1\rangle = \begin{pmatrix} \cos(\theta) \\ \sin(\theta) \end{pmatrix} = \cos(\theta)\,|\Psi_+\rangle + \sin(\theta)\,|\Psi_-\rangle \qquad E_1 = \frac{E}{2} = \frac{1}{2}\sqrt{\Delta^2 + \Delta_0^2}$$
$$|\Psi_2\rangle = \begin{pmatrix} \sin(\theta) \\ -\cos(\theta) \end{pmatrix} = \sin(\theta)\,|\Psi_+\rangle - \cos(\theta)\,|\Psi_-\rangle \qquad E_2 = -\frac{E}{2}$$

1.3.2 Relevant parameters and limiting cases

We observe here that the matrix elements $A_{L,R}$ and $\delta V_{L,R}$, and therefore Δ_0, are in principle dependent on the explicit form of the potential. We obtain a result that is independent of such microscopic details by adding two additional hypotheses:

- the barrier is wide: $\delta \gg x_w$. Then

$$A_L \coloneqq \langle\Psi_L|V - V_L|\Psi_L\rangle \approx \frac{x_w^4}{32}V^{(4)}(x_L)$$
$$A_R \coloneqq \langle\Psi_R|V - V_R|\Psi_R\rangle \approx \frac{x_w^4}{32}V^{(4)}(x_R)$$
$$S\delta V_L \coloneqq \langle\Psi_R|V - V_L|\Psi_L\rangle \approx S(V(\overline{x}) - V_L(\overline{x})) \qquad \overline{x} \coloneqq \frac{x_L + x_R}{2}$$
$$S\delta V_R \coloneqq \langle\Psi_L|V - V_R|\Psi_R\rangle \approx S(V(\overline{x}) - V_R(\overline{x}))$$

- $\overline{x} \approx 0$, which is a request for good spacial symmetry. Then $V(\overline{x}) \approx V(0) = V$ and

$$\Delta_0 = 2S\overline{\delta V} = S(\delta V_L + \delta V_R) \approx S\Big(V - \frac{\hbar\omega_w}{2}\frac{\delta^2}{4x_w^2}\Big)$$

Under these assumptions the whole hamiltonian only depends on a few parameters: the distance δ, the characteristic pulse ω_w, the asymmetry Δ and the barrier height V.

To verify the coherence of the results so far, it is useful to consider the following limiting cases:

- $S \to 0 \implies \Delta_0 \to 0$. In the limit of very large δ the overlap integral S vanishes. We expect tunneling to be impossible in this limit, which can then be interpreted as a classical limit in which quantum mechanical effects are negligible. We would have $H_0 = \Delta/2\sigma_x$ in the $|\Psi_\pm\rangle$ basis, so the eigenfunctions of H_0 would simply be the single well ground states Ψ_L and Ψ_R with energy $\pm\Delta/2$;

- $\Delta \to 0$. This is the particular case of an exactly symmetric potential. We would have $H_0 = \Delta_0/2\sigma_z$, diagonal in the $|\Psi_\pm\rangle$ basis. The eigenfunctions are then $\Psi_\pm$, the symmetric and anti-symmetric combinations of the single well ground states. This is not unexpected: if the potential is symmetric the eigenvectors of H_0 are also parity eigenvectors.

1.3.3 Interaction with a phonon

As already seen in section 1.2, the perturbing potential $V_e(x,t)$ is, in first order approximation, spacially anti-symmetric. In the $|\Psi_\pm\rangle$ basis of parity eigenvectors, the perturbation is completely off-diagonal:

$$H = H_0 + H_{ext} = \frac{1}{2}\begin{pmatrix}\Delta_0 & \Delta \\ \Delta & -\Delta_0\end{pmatrix} + \begin{pmatrix}0 & 1 \\ 1 & 0\end{pmatrix}\gamma e(t)$$

where we have used $\gamma \coloneqq \frac{1}{2}\frac{\partial\Delta}{\partial e}$ as defined in section 1.2.

In the basis $|\Psi_{1,2}\rangle$ of eigenvectors of H_0:

$$\begin{aligned} H = H_0 + H_{ext} &= \frac{1}{2}\begin{pmatrix}E & 0 \\ 0 & -E\end{pmatrix} + \begin{pmatrix}\sin(2\theta) & -\cos(2\theta) \\ -\cos(2\theta) & -\sin(2\theta)\end{pmatrix}\gamma e(t) \\ &= \frac{1}{2}\begin{pmatrix}E & 0 \\ 0 & -E\end{pmatrix} - \frac{1}{2}\begin{pmatrix}-D & 2M \\ 2M & D\end{pmatrix}e(t) = \frac{1}{2}\big(E + De(t)\big)\sigma_z - Me(t)\sigma_x \end{aligned}$$

with $D = 2\frac{\Delta}{E}\gamma$ and $M = \frac{\Delta_0}{E}\gamma$.

This hamiltonian is equivalent to that of a spin 1/2 in a constant magnetic field along the z direction and perturbed by an additional time dependent magnetic field: the unitary time evolution of the system would resemble the resonant rotation of a spin in a magnetic field described by the Bloch equations, in the absence of the relaxation term. However, we are not interested in the unitary time evolution of the system, but in the statistical non-unitary evolution of a collection of such states when coupled with an external bath. Let ρ be the density matrix of the (mixed) state: its time evolution will follow the Lindblad master equation

$$\frac{d\rho}{dt} = -\frac{i}{\hbar}\big[H,\rho\big] + \frac{1}{\tau_{12}}\Big(L_{12}^\dagger\rho L_{12} - \frac{1}{2}\big\{L_{12}^\dagger L_{12},\rho\big\}\Big) + \frac{1}{\tau_{21}}\Big(L_{21}^\dagger\rho L_{21} - \frac{1}{2}\big\{L_{21}^\dagger L_{21},\rho\big\}\Big) \tag{1.6}$$

where L_{12} and L_{21} are jump operators that allow the system to "jump" or relax between the two states and τ_{12} and τ_{21} are the inverse frequencies of the two jumps,

$$\begin{aligned} L_{12} &= |\Psi_2\rangle\langle\Psi_1| & \tau_{12}(t) &= \tau_0 e^{\beta V} e^{\frac{\beta}{2}(E+De(t))} \\ L_{21} &= |\Psi_1\rangle\langle\Psi_2| & \tau_{21}(t) &= \tau_0 e^{\beta V} e^{-\frac{\beta}{2}(E+De(t))} \end{aligned}$$

using for τ_{12} and τ_{21} the classical result already used in 1.2, euristically substituting $E + De(t)$ to $\Delta + 2\gamma e(t)$ as the splitting between the two levels.

Using the parametrisation $\rho(t) = \begin{pmatrix} p(t) & a(t)+ib(t) \\ a(t)-ib(t) & 1-p(t) \end{pmatrix}$ equation 1.6 becomes:

$$\begin{cases} \dot{p}(t) = -\frac{1}{\tau(t)}(p(t) - p_{eq}(t)) - \omega_M b e(t) & \omega_M = \frac{2M}{\hbar} \\ \dot{a}(t) = -\frac{1}{2\tau(t)}a(t) + (\omega_0 + \omega_D e(t))b(t) & \omega_0 = \frac{E}{\hbar} \\ \dot{b}(t) = -\frac{1}{2\tau(t)}b(t) - (\omega_0 + \omega_D e(t))a(t) + \omega_M\big(p - \frac{1}{2}\big)e(t) & \omega_D = \frac{D}{\hbar} \end{cases}$$

where $\tau(t) = \tau_0 e^{\beta V}\operatorname{sech}\big(\frac{\beta}{2}(E+De(t))\big)$ and $p_{eq}(t) = \frac{1}{2}\big(1+\tanh\big(\frac{\beta}{2}(E+De(t))\big)\big)$, just like in section 1.2.

Defining again $q(t) = p(t) - p_{eq}$ and keeping only first order terms in $e \ll 1$ (again considering that a, b and q are asymptotically of order e) we get

$$\begin{cases} \dot{q}(t) = -\frac{1}{\tau}q(t) + \frac{q_D}{\tau}e(t) & q_D = \frac{\beta D}{4}\operatorname{sech}^2(\frac{\beta}{2}E) \\ \dot{a}(t) = -\frac{1}{2\tau}a(t) + \omega_0 b(t) & \\ \dot{b}(t) = -\frac{1}{2\tau}b(t) - \omega_0 a(t) + \frac{\omega_M}{2}\tanh\big(\frac{\beta}{2}E\big)e(t) & \end{cases}$$

The solution for $e(t) = e_0 e^{i\omega t}$ is

$$\begin{aligned} q(t) &= \chi_z e(t) = \frac{q_D}{1+i\omega\tau}e(t) \\ a(t) &= \chi_x e(t) = \frac{2\omega_M\omega\tau^2}{1+(2\omega_0\tau)-(2\omega\tau)+4i\omega\tau}\tanh\big(\frac{\beta}{2}E\big)e(t) \\ b(t) &= \chi_y e(t) = \frac{\omega_M\tau(1+2i\omega\tau)}{1+(2\omega_0\tau)-(2\omega\tau)+4i\omega\tau}\tanh\big(\frac{\beta}{2}E\big)e(t) \end{aligned}$$

χ_z and χ_x are the longitudinal and transverse dynamical susceptibility, defined in analogy with the magnetisation problem.

1.3.4 Loss angle

We can now compute the two-level system's contribution to the elastic modulus:

$$\begin{aligned} \delta U(T,p,a,e) = \langle H\rangle = Tr(\rho H) &= \frac{1}{2}(E+De)(2p-1) - 2Mae \\ \begin{cases} \frac{\partial(\delta\sigma)}{\partial p} &= D \\ \frac{\partial(\delta\sigma)}{\partial a} &= -2M \end{cases} &\implies \delta\sigma = Dq - 2Ma = (D\chi_z - 2M\chi_x)e \\ \delta\mathcal{E} = \frac{\delta\sigma}{e} &= D\chi_z - 2M\chi_x \end{aligned}$$

In order to compare this result with the classical one it is convenient to remember $D = 2\gamma\frac{\Delta}{E}$ and $M = \frac{\Delta_0}{E}\gamma$:

$$\delta\mathcal{E} = 2\frac{\Delta}{E}\gamma\Big(\chi_z - \frac{\Delta_0}{\Delta}\chi_x\Big)$$

We obtained this result with a quantum mechanical approach that accounts for coherence, and find

that there are two contributions to the elastic modulus for each TLS. The first term

$$\delta\mathcal{E}_{rel} = 2\frac{\Delta}{E}\gamma\chi_z$$
$$\delta Q^{-1}_{rel} = \frac{Im(\delta\mathcal{E}_{rel})}{Y} = \Big(\frac{\Delta}{E}\Big)^2 \frac{\gamma^2}{k_B T Y}\frac{\omega\tau}{1+(\omega\tau)^2}\mathrm{sech}^2\Big(\frac{\beta}{2}E\Big)$$

arises from the relaxation process. It is the generalisation of the classical result obtained before: by taking the classical limit $S \to 0$ (the limit in which tunneling is impossible) we have $\Delta_0 \to 0$, $E \to \Delta$ and thus we find again the classical result.

The second term

$$\delta\mathcal{E}_{res} = -2\frac{\Delta_0}{E}\gamma\chi_x$$
$$\delta Q^{-1}_{res} = \frac{Im(\delta\mathcal{E}_{res})}{Y} = \frac{4M\tau}{\hbar Y}\frac{4\omega_0\omega\tau^2}{(1+(2\omega_0\tau)^2+(2\omega\tau)^2)^2}\tanh\Big(\frac{\beta}{2}E\Big)$$

arises from coherent processes. It is purely quantum mechanical: in the classical limit $\Delta_0 \to 0$ and the term vanishes. This resonance term shows a peak at $\omega = \omega_0\sqrt{1+\frac{1}{(2\omega_0\tau)^2}} \xrightarrow{T\to 0K} \omega_0$.

The expected loss angle of the material is obtained by integrating over the TLS parameters.

Chapter 2

In silico two-level system search in amorphous tantala

In this chapter we present the results of our TLS search in simulated samples of amorphous tantala. We assume the physical realisations of two-level systems to be pairs of local minima of the potential energy in configuration space, separated by a saddle. Our goal is then to look for such configurations in realistic models of amorphous tantala, generated using LAMMPS MD software [13].

Once we have identified a set of TLSs we compute the loss angle for mechanical dissipation using equation 1.5: at temperatures higher than a few Kelvin the resonance term is negligible and thus the classical result may be used.

2.1 Methodology: event search and TLS identification

Sample preparation To prepare a sample the Ta_2O_5 crystal structure is first equilibrated at 300 K in an NVT ensemble for 50 ps, then melted to 5000 K in 140 ps using an NPT ensemble. The sample is again equilibrated for 50 ps before being quenched to 300 K in 140 ps, for a quench rate of 35.6 K/ps, using an NPT ensemble. After a final 50 ps of relaxation the energy is minimised and the final configuration is saved as a sample.

Event search with ART We generated 325 samples of 336 atoms, and on each performed 150 event searches with pARTn [12], the latest implementation of the activation-relaxation technique. The algorithm explores the potential energy landscape around the configuration of each sample: starting from an initial minimum it pushes the system out of its basin (*activation*) towards a saddle configuration *sad* and then relaxes from the saddle in both directions (*relaxation*), minimising the energy and obtaining two configurations min_1 and min_2. We call an event each 3-tuple of configurations (min_1, *sad*, min_2): each event is a candidate two-level system.

We must note here that

- the same two-level system may be found multiple times by the search algorithm, resulting in physically equivalent events. The treatment of equivalent events is discussed in the next paragraph.

- since the potential landscape is rugged, not every event found by pARTn corresponds to a physical two-level system: in many cases the algorithm finds saddles or minima that are only a result of the rugged nature of the potential. We shall call this events *non-physical*: in this category also fall events that are clearly pARTn failures, like events in which the saddle point has lower energy than a minimum.
- the forward and backward relaxations may fall into the same basin, resulting once again in non-physical events, since there is no significant movement of the system between the two configurations.

To avoid events in which the initial and final configuration are in the same basin of attraction we consider only events in which the two minima are separated by more than 1 Å in configuration space. Similarly, we only consider events in which the saddle point has higher energy than both minima.

Identifying TLSs: equivalent events Two events are said to be *equivalent* if they correspond to the same physical two-level system, so if they connect the same two basins. To determine whether two events are equivalent we use both a maximum distance cutoff between the configurations as well as a minimum cutoff on the scalar product between the directions of the movements in configuration space. We observe that this additional requirement greatly improves the accuracy of the discrimination between pairs of equivalent events and pairs of non-physical events that are by chance close-together. Let us call *cluster* each equivalency class identified using these criteria. Observing that there is no physical distinction between a given event and the one obtained from it by swapping the initial and final configurations, this scalar product is also useful to recognize and flip these events so that they are correctly clustered.

We exploit the existence of equivalent events for two purposes: to distinguish physical events from non physical events; and to compute averaged properties of the underlying two-level system.

We assume that two non-physical events have a much lower probability being clustered than physical ones: we choose then to only consider clusters that include more then one event. The choice of this cutoff is not unique and is dependent on the number of total searches.

TLS properties For each cluster we define a two-level system whose properties are computed as the mean properties of the events in the cluster.

For simplicity we consider the attempt rate as constant $\frac{\tau_0}{2} = 0.5$ ps. For a more thorough calculation, one would need to compute τ_0 for each events using the eigenvalues of the hessian matrix of the potential at the minima and at the saddle [2] [14]. It has been shown, however, that the simplification does not dramatically affect the final result [2]. The only parameters needed to compute the loss angle using equation 1.5 are then: barrier height V, asymmetry Δ and deformation potential γ.

For V and Δ we use the mean values of the energies at the minima and at the saddle computed across all events in the cluster.

The deformation potential was defined in section 1.2 as $\gamma = \frac{1}{2}\frac{\partial \Delta}{\partial e}$, where e is the strain applied to the system. The direction of the applied strain was chosen arbitrarily and should not have any effect on the result, provided that the simulation box is big enough to capture the long range disorder of the amorphous material. Using this definition we calculated γ for each event by applying different

Figure 2.1: Distribution of the TLS parameters. From left to right: barrier height V and asymmetry Δ; number of active Ta and O atoms; distance between the two minima δ and displacement of the most active atom δ_{max}; number of bonds formed and broken by active atoms

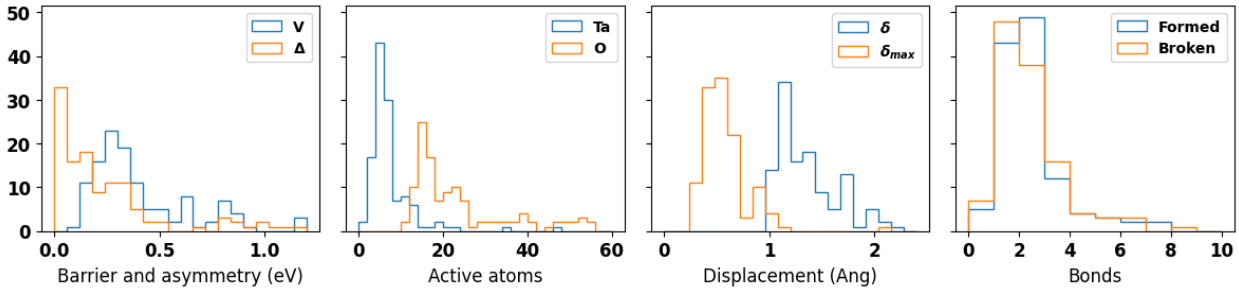

values of strain to the two minima configurations and computing the slope of the asymmetry as a function of the strain.

Other interesting features calculated for every event are: the distance δ between the two minima; the displacement of the most active atom δ_{max}; the number of active atoms and the number of bonds broken and formed by active atoms. The minimum displacement for an atom to be considered active is 0.1 Å. Two atoms are considered bonded if their distance is less then 2.55 Å, and not bonded if it is more then 2.65 Å.

2.2 TLS analysis and classification

2.2.1 Density of TLS

The number of distinct TLS found was 121, for a density of 1.1 per 1000 atoms or 0.088 nm^{-3}, which is in accord with previos in silico searches [2][10].

This estimate depends of the criteria used for clustering and for defining TLSs. More importantly, the number of TLSs found depends on the search algorithm's sensibility. In our case, pARTn is best at identifying events with activation energies between 0.1 and 1 eV. We can imagine there are many events with lower activation energies: these, however, do not contribute significantly to dissipation in the range of frequency and temperature considered, as will be shown in the next paragraph.

2.2.2 Barrier and asymmetry distribution

Figure 2.1 is a summary of the properties of the two-level systems found. Typical TLSs have 20 to 40 active atoms and 0 to 10 total bonds involved. The total displacement ranges form 1 to 2 Å, the displacement of the most active atom accounting for approximately half of the total.

As anticipated in the previous paragraph, the search algorithm does not find events with very low activation energies. The barrier and asymmetry distributions are then expected to not be accurate for very small values of V and Δ.

In figure 2.2 each TLS is shown in the (V, Δ) plane as a circle whose size scales logarithmically with its maximum dissipation. Expanding some observations already made in section 1.2 we find that:

- TLS with high asymmetry (indicatively $\Delta > V/3$, outside of the inner dotted lines in figure 2.2) have very low dissipation;

Figure 2.2: Barrier and asymmetry of each TLS. Size scales logarithmically with the TLS's maximum dissipation. On the left, color represents T_{max}, the temperature of highest dissipation (for $f = 1$ kHz), on the right the frequency of maximum dissipation f_{max} (for $T = 300$ K).

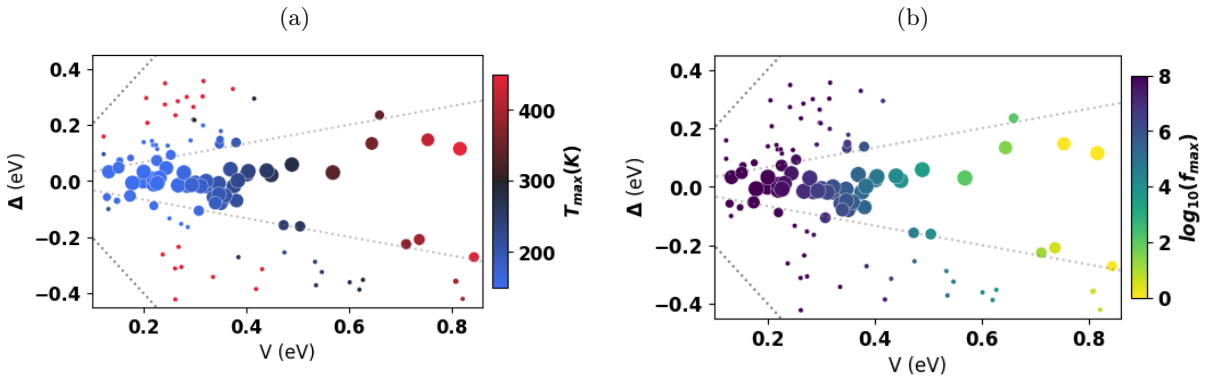

Figure 2.3: Total and maximum displacement for each TLS. Size scales logarithmically with the TLS's maximum dissipation, while color represents the number of active atoms (2.3a) or bonds (2.3b), or the temperature of maximum dissipation (2.3c).

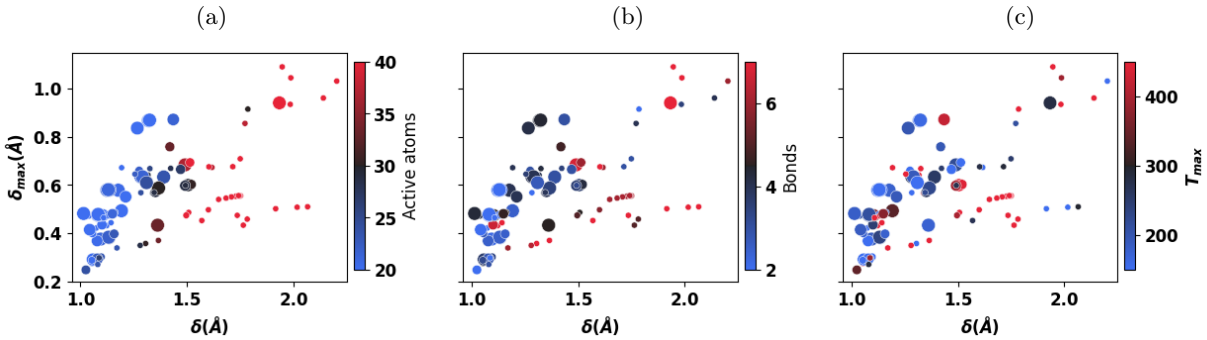

- TLS whose peak dissipation (at a fixed $f = 1$ kHz) occurs near room-temperature have barriers between 0.4 and 0.6 eV (see figure 2.2a), higher barriers corresponding to higher temperatures;
- TLS whose peak dissipation (at a fixed $T = 300$ K) occurs for frequency between 10 Hz and 10 kHz have barriers between 0.5 and 0.7 eV (see figure 2.2b), higher barriers corresponding to lower frequencies.

2.2.3 Topological analysis

To gain further insight on the microscopical nature of the TLSs, let us examine the correlation between the total displacement δ between the two minima and the displacement of the most active atom δ_{max}. In figure 2.3 we can see that there is, as expected, some correlation between the two. This correlation, however, is not perfect: for a fixed maximum displacement δ_{max} there is a wide range in the total displacement δ observed. The intuition that events with higher δ and lower δ_{max} should involve more active atoms is confirmed in figure 2.3a, in which TLSs are colored according to the number of active atoms. From further analysis we see that other features also show a similar correlation with δ and δ_{max}: among these the number of bonds involved, the maximum dissipation and the temperature of maximum dissipation (see figure 2.3).

In light of these regularities, which point to the distinction of TLSs in two classes, it is natural to ask if they have a microscopical origin, i.e. if the two sets of events arise from two essentially

Figure 2.4: Events A (left) and B (right). The initial and final configurations are shown side by side, on the (x, y) plane; the size of the atoms is proportional to z; active atoms are opaque (blue for Ta, orange for O) and arrows represent the movements of the atoms whose displacement is more that 0.2 Å; only bonds between active atoms are shown, and broken and formed bonds are highlighted in red and green.

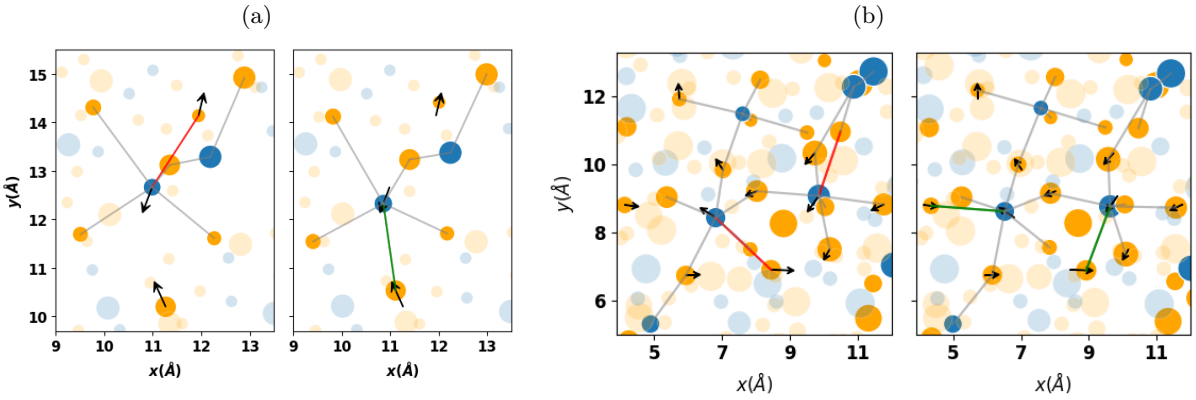

different types of microscopical movements. Let us define a TLS to be of type **A** if it has less then 25 active atoms, and **B** otherwise. With this definition the two classes contain roughly the same number of TLSs.

Let us consider two events chosen to belong two these two classes. In figure 2.4 the initial and final configurations are shown side by side; configurations are projected in the (x, y) plane, while the third dimension is rendered through the size of the atoms; only active atoms are opaque (blue for Ta, orange for O), and arrows are added to represent the movements only of the atoms whose displacement is more that 0.2 Å; only bonds between active atoms are shown, and broken and formed bonds are highlighted in color.

The first event, which we will call A, is shown in figure 2.4a: the central tantalum atom breaks a bond with an oxygen atom, and forms a new one with another oxygen. This is an example of a bond-hopping event [10]: it involves the diffusion of a coordination defect, and is made possible by the movement of a single atom, leading to the relaxation of the neighbors.

Event B, in figure 2.4b, is much more complicated as it features many atoms moving considerably. Among these we can see a chain of three Ta atoms exchanging oxygen bonds. This event might be interpreted as a bond-exchange TLS [10]: the two central Ta atoms, the most active, exchange neighbors while the distance between them does not change considerably.

Notably, there is a significant difference in the asymmetry distribution between the two classes: from figure 2.5 we see that systems of type A have generally very low asymmetry, to the point that all events with asymmetry higher than 0.5 eV are of type B. This distinction can also be seen to some degree in the barrier distribution. It is interesting to notice that analogous differences in the barrier distribution where observed between bond-defect-hopping and bond-exchange events in SiO_2 [10], suggesting some kind of common features between different materials, simulated with very different interatomic potentials.

Finally, we note that the majority of top dissipating systems belong to the first category or class: of the 30 TLS with highest dissipation at 300 K and 1 kHz, 25 have less then 25 active atoms. Events outside of these 30 have negligible dissipation, at least at this temperature and frequency: their contribution is more then 1000 times smaller then that of the systems with highest dissipation.

Figure 2.5: Distribution of the TLS barrier (left) and asymmetry (right) for events of type **A** and **B**

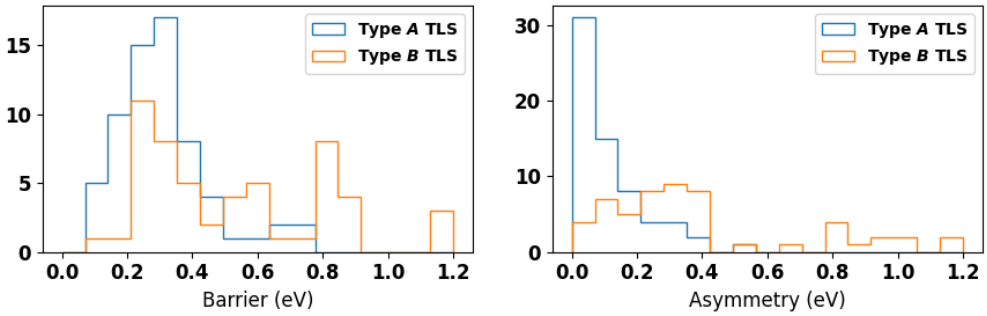

2.2.4 Deformation potential

The deformation potential γ measures how strongly each system is coupled to incoming mechanical waves. These have both direction and polarisation, hence it would be more precise to regard γ as a tensor. Here, however, we only consider longitudinal waves propagating in an arbitrarily chosen direction, thus γ is effectively a scalar.

The deformation potential of a system as defined here obviously depends on the random direction chosen for the perturbation, and consequently so does its contribution δQ^{-1} to the loss angle, which is proportional to γ^2 (see equation 1.4). In an ideal infinite sample of amorphous material (or even in a finite macroscopic sample) we would expect to find infinitely many occurrences of similar events, each with a different orientation. The resulting dissipation would then be independent on the wave's direction. In our case we only have a few events: as we shall see in section 2.3 our results greatly depend on the contributions of single TLSs. We would hope to obtain an averaging effect similar to having a much larger sample by using a mean value of γ^2.

The average square deformation potential obtained across all TLSs (see figure 2.6) is

$$\langle \gamma^2 \rangle_{ALL} \approx 276 \text{ eV}^2$$

This value is an order of magnitude higher than the one obtained by Trinastic et al [14] on Ta_2O_5. The comparison, however, is not very significant as the set of TLS studied is different: in the cited work, in which standard molecular dynamics is used for the search, the bulk of the TLSs found have barriers lower than 0.1 eV, while our search method allowed us to only find events with much higher barrier (see figure 2.1). As already pointed out by Damart et al [2] to explain the discrepancy between their average deformation potential and the experimental value for SiO_2 (both are shown in figure 2.6), events with much lower barriers are expected to have lower values of γ.

The deformation potential, however, may also depend on the system's microscopical details, and not only on its orientation. This is indeed the case: the mean square value calculated using only the 30 most dissipating systems (labeled HD for high dissipation) is significantly different that the values obtained using the other TLSs (LD, low dissipation), indicating some correlation between the TLS's properties and the deformation potential:

$$\langle \gamma^2 \rangle_{HD} = (125 \pm 26) \text{ eV}^2$$
$$\langle \gamma^2 \rangle_{LD} = (326 \pm 51) \text{ eV}^2$$

Figure 2.6: Square longitudinal deformation and barrier height for each TLS. The average value $\langle\gamma^2\rangle$ is shown along with values obtained in previous works on SiO_2 and Ta_2O_5 (D for Damart et al [2], T for Trinastic et al [14]), and the experimental value for SiO_2; no experimental value is known for Ta_2O_5.

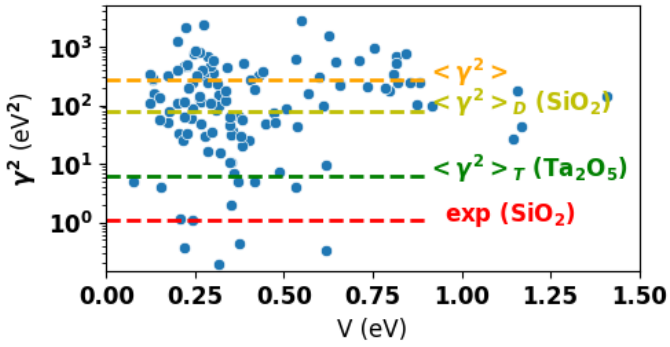

These averages are not compatible with very high confidence: the gaussian compatibility between the two is 3.5. Having verified that the most dissipating events at any temperature and frequency of interest are among these 30, in the following we will use $\langle\gamma^2\rangle_{HD}$ as an estimate of the average deformation potential for all averaged loss angle calculations.

2.3 Loss angle

Using equation 1.5 we can compute the total loss angle at any temperature and frequency. In figure 2.7a we show in blue the result for the total loss angle, while the pale lines show the single TLSs' contributions. With this few data (the total number of systems found is just 121) the result has not yet converged and big fluctuations due to single TLSs are visible. We obtain a smoother line by assuming the mean value $\langle\gamma^2\rangle$ as the square deformation potential for each system instead γ_i^2 (see figure 2.7a. In the following we always use this assumption, which has been shown to have little effect on the loss angle calculation [2].

2.3.1 Qualitative analysis

Our calculation captures some of the features observed in experimental data. At room temperature, dissipation is greater at higher frequencies [6]. This trend is clear in figure 2.7, even though our result shows a stronger frequency dependence then experimentally observed. In figure 2.7c this observation is further examined by showing the loss angle as a function of temperature for different frequencies: after a low temperature peak, dissipation diminishes at higher temperatures and above 200 K lower frequencies are associated with lower dissipation. This finds confirmation both in previous in silico calculations [14] and in experimental measurements [11].

Some additional observations can be made from our results, in particular regarding the link between the microscopical details of the TLSs and their dissipation: figure 2.7b shows that most of the dissipation comes from systems with relatively few bonds involved and active atoms, similar to event A in section 2.2.3. We had already made a similar observation in section 2.2.3 regarding dissipation at 300 K and 1 kHz, however figure 2.7b extends its validity to a much wider range of temperature and frequency. Note that the cutoff values of 25 atoms and 10 bonds are chosen so that in both cases the two sets of TLS contain half the total number of systems.

Figure 2.7: Loss angle as a function of frequency (left) or temperature (right).

(a)

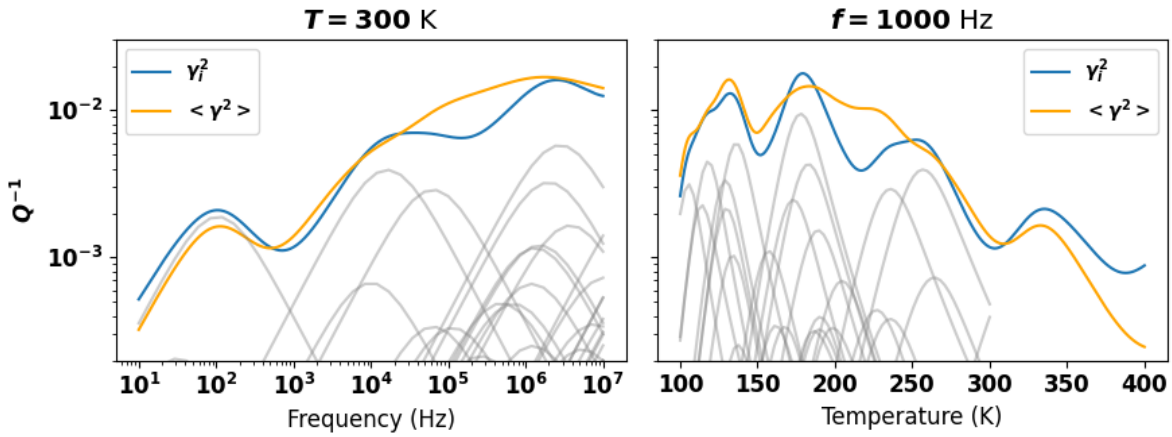

(b)

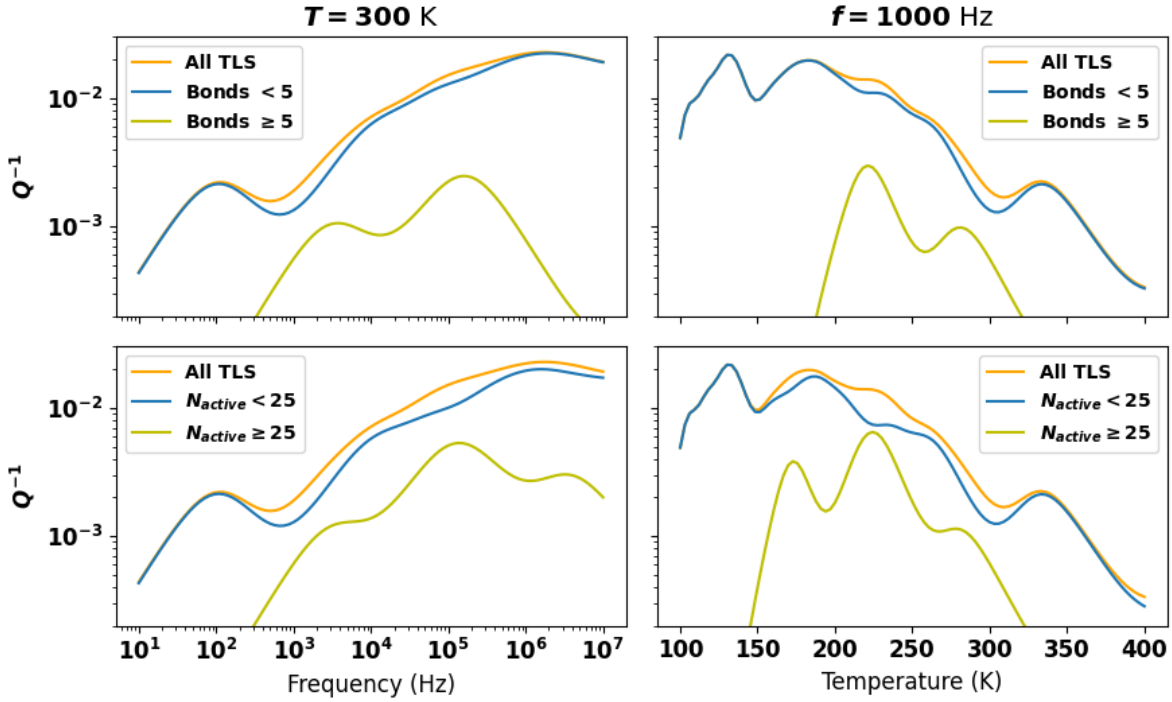

(c)

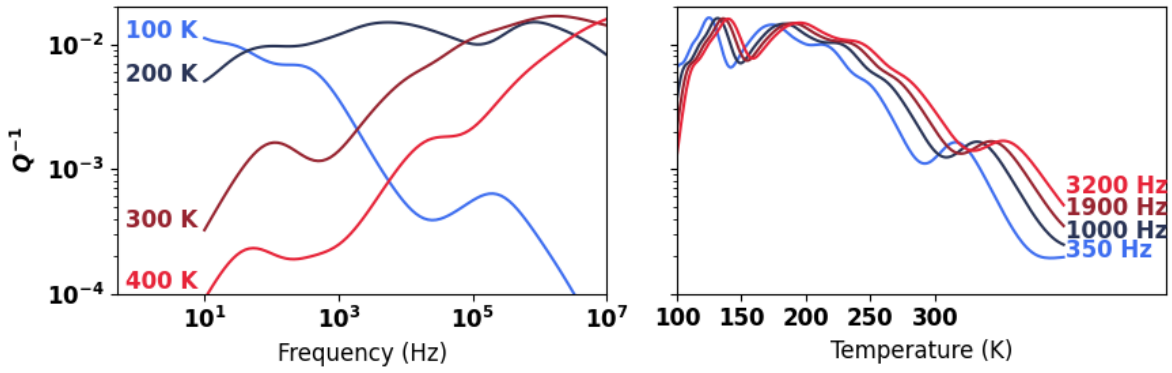

2.3.2 Quantitative comparison with experimental data

As a reference for experimental measurements of the loss angle in Ta_2O_5 coatings we use the results obtained on those provided by the Laboratoire des Matériaux Avancés (LMA) for the VIRGO gravitational interferometer [4].

The computed loss angle at room temperature is higher than experimental values obtained on annealed samples: reported values grow from 4×10^{-4} at 1 kHz to 5×10^{-4} at 20 kHz, while our result is 3 to 10 times as large. These samples, however, are annealed or heat treated to reduce dissipation: heat treating the Ta_2O_5 coatings at different temperatures has been shown [15] to significantly reduce loss angle. Simulations, on the other hand, cannot account for this relaxation process, which occurs over macroscopic time scales (samples are annealed for hours and then are allowed to cool very slowly). Quantitative comparison with experimental data for not annealed Ta_2O_5 [15][5] shows a better agreement, giving approximately the same value at 1 kHz and a value that is 5 times as large at 12 kHz.

Conclusions

In this thesis work we have applied activation-relaxation-technique (ART) to two-level system search in realistic models of amorphous Ta_2O_5 in order to estimate the loss angle of the material: this was the first time the method has been applied to tantala.

We generated 325 samples of Ta_2O_5 and performed almost 50000 event searches with pARTn. We analysed the events in order to identify physical and distinct two-level systems and found 121 such systems, for a density similar to those found in previous works on amorphous SiO_2. We then studied the properties of these TLSs, focusing on the activation barrier's height and asymmetry and on the active atoms: their number, their displacements and their bonds. In particular, we were interested in how these microscopic features may be related to dissipation.

Finally we computed the loss angle of Ta_2O_5 as a function of temperature and frequency, applying the prediction of the TLS model to the set of two-level systems found. The result is in qualitative accord with experimental data, and also in reasonable quantitative agreement, at least in the range of temperature and frequency of interest. This demonstrates once again the validity of the TLS model that motivates the current efforts into the numerical study of dissipation in glasses, ultimately with the intent of directing the research for new materials that minimize thermal noise. It also testifies to ART as a promising alternative to classical molecular dynamics methods for TLS search in amorphous materials; this is especially true for TLSs with high activation energies, which are the most difficult to find using molecular dynamics but also the most important for dissipation close to room temperature.

Our microscopic characterisation allowed us to make some additional observations, in particular that, for a wide range of temperatures and frequencies, the two-level systems that account for most of the dissipation are those with relatively few active atoms and bonds involved. We suggested a possible distinction between two different classes of systems, which also show very different distribution of barrier height and asymmetry. Further analysis would be needed to confirm the identification of these two classes with bond-hopping TLS and bond-exchange TLS, observed in amorphous SiO_2.

Possible ways of extending and refining these results include the optimisation the force fields used, which could improve quality and reliability of the TLS search, as well as the increase in both sample size and number of searches. The former would allow for longer wavelength excitations, possibly extending the validity of the final result to lower temperatures, while the latter would grant better convergence of the loss angle calculation. At the same time, experimenting with different initial pushes for pARTn could improve its efficiency and rule out any possible biases of the search algorithm. Once the method is refined, it may be used on different materials, such as titania doped tantala, or on differently prepared samples in order to investigate how this affects the distribution

of two-level systems and the final result for dissipation. Finally, it might be worthwhile to combine different search methods to complement their strengths: while ART is better suited to calculate dissipation at room temperature and relatively low frequencies, other methods based on molecular dynamics give better results at cryogenic temperatures or very high frequencies.

Bibliography

[1] G.T Barkema and Normand Mousseau. "The activation–relaxation technique: an efficient algorithm for sampling energy landscapes". In: *Computational Materials Science* (2001).

[2] T. Damart and D. Rodney. "Atomistic study of two-level systems in amorphous silica". In: *Phys. Rev. B* (2018).

[3] K. S. Gilroy and W. A. Phillips. "An asymmetric double-well potential model for structural relaxation processes in amorphous materials". In: *Philosophical Magazine B* (1981).

[4] M Granata et al. "Amorphous optical coatings of present gravitational-wave interferometers". In: *Classical and Quantum Gravity* (2020).

[5] M. Granata et al. "Internal Friction and Young's Modulus Measurements on SiO2 and Ta2O5 Films Done with an Ultra-High Q Silicon-Wafer Suspension". In: *Archives of Metallurgy and Materials* (2015).

[6] Gregory M Harry and (forthe LIGO Scientific Collaboration). "Advanced LIGO: the next generation of gravitational wave detectors". In: *Classical and Quantum Gravity* (2010).

[7] J. Jäckle et al. "Elastic effects of structural relaxation in glasses at low temperatures". In: *Journal of Non-Crystalline Solids* (1976).

[8] H.A. Kramers. "Brownian motion in a field of force and the diffusion model of chemical reactions". In: *Physica* (1940).

[9] Paul Langevin. "Sur la théorie du mouvement brownien". In: *Compt. Rendus* (1908).

[10] Carl Lévesque et al. "Internal mechanical dissipation mechanisms in amorphous silicon". In: *Phys. Rev. Mater.* (2022).

[11] I W Martin et al. "Effect of heat treatment on mechanical dissipation in Ta2O5 coatings". In: *Classical and Quantum Gravity* (2010).

[12] M. Poberznik et al. "pARTn: A plugin implementation of the Activation Relaxation Technique nouveau that takes over the FIRE minimisation algorithm". In: *Computer Physics Communications* (2024).

[13] Aidan P. Thompson et al. "LAMMPS - a flexible simulation tool for particle-based materials modeling at the atomic, meso, and continuum scales". In: *Computer Physics Communications* (2022).

[14] Jonathan P. Trinastic et al. "Molecular dynamics modeling of mechanical loss in amorphous tantala and titania-doped tantala". In: *Phys. Rev. B* (2016).

[15] G Vajente et al. "Effect of elevated substrate temperature deposition on the mechanical losses in tantala thin film coatings". In: *Classical and Quantum Gravity* (2018).

Appendix A

Kramer's escape time

A.1 Brownian motion

Brownian motion (in one dimension) describes how a mesoscopic particle moves in a one-dimensional fluid at thermal equilibrium at a temperature T under an external potential $U(x)$. We usually follow Langevin [9] and model the effect of the many collisions with the particles of the fluid as the sum of a deterministic friction force and some "white" noise, i.e. a δ-correlated, homogeneous and isotropic stochastic addition. In our specific case we choose the friction to be proportional to the velocity and the noise to be Gaussian. We treat the motion of the particle as a stochastic process in phase-space $(X(t), V(t))$ with increments:

$$\begin{cases} \Delta X = V(t)\Delta t \\ \Delta V = \left(\frac{-\partial_x U(X(t),t)}{m} - \frac{\alpha}{m}V(t)\right)\Delta t + \sqrt{\frac{2\alpha}{\beta m^2}}\Delta\hat{W} \end{cases} \tag{A.1}$$

where $\Delta\hat{W} = \hat{W}(\Delta t)$ is a normalised Wiener process at time Δt. The dependence of the amplitude of the noise on the temperature is a consequence of the fluctuation-dissipation theorem. We will denote with $p(x, v, t|x_0, v_0, 0)$ the probability density in phase-space for a particle with $(X(0), V(0)) = (x_0, v_0)$. For brevity of notation and to make the equations more readable I will use $p(x, v, t)$ and sometimes even p instead of $p(x, v, t|x_0, v_0, 0)$. The Fokker-Plank equation associated with the stochastic sistem A.1 is

$$\partial_t p = -\partial_x(vp) + \partial_v\big(\frac{\alpha}{m}vp + \frac{\partial_x U}{m}p\big) + \frac{\alpha}{\beta m^2}\partial^2_{vv}p \tag{A.2}$$

known as Kramers' equation.

Our goal is to obtain an equation for the probability density in real-space

$$\rho(x,t) \coloneqq \int_{-\infty}^{+\infty} p(x,v,t)\,dv \qquad\qquad j(x,t) \coloneqq \int_{-\infty}^{+\infty} vp(x,v,t)\,dv$$

Integrating A.2 and using $p(x,v,t) \xrightarrow{v\to\infty} 0$ we get

$$\partial_t \rho(x,t) = -\partial_x \int_{-\infty}^{+\infty} v p(x,v,t)\, dv =: -\partial_x j(x,t) \tag{A.3}$$

$$\partial_t j(x,t) = -\partial_x \int_{-\infty}^{+\infty} v^2 p(x,v,t)\, dv - \frac{\alpha}{m} j(x,t) - \frac{\partial_x U(x,t)}{m}\rho(x,t) \tag{A.4}$$

a complete set of coupled equations for $\rho(x,t)$ and $j(x,t)$. To perform the integral left in A.4 we would need some hypothesis on $p(x,v,t)$.

A.2 The over-damped limit: Smoluchowski's equation

In the high friction limit the effect of the Brownian forces on the velocity of the particle is much larger then the external force acting on it, so the particle can thermalize very fast with the fluid at temperature T. We will formally take this limit by performing an expansion for small m, observing that if we keep $\alpha = \gamma m$ constant in the limit for $\gamma \to +\infty$ we have $m \to 0$. In this over-damped limit we expect the distribution of the velocities to be close to a Maxwell-Boltzmann distribution:

$$p(x,v,t) \approx N e^{-\frac{\beta m}{2} v^2} \rho(x,t) \qquad\qquad N = \sqrt{2\pi/\beta m}$$

This is indeed the approach originally taken by Kramers in 1940 [8]. We realise, however, that Kramers' approximation is not self-consistent, as we would get

$$j(x,t) = \int_{-\infty}^{+\infty} v p(x,v,t)\, dv \approx N\rho(x,t) \int_{-\infty}^{+\infty} v e^{-\frac{\beta m}{2} v^2}\, dv = 0$$

a null probability current, which means a stationary probability density in real-space. To avoid this we consider a velocity distribution close to a Maxwell-Boltzmann but locally shifted

$$p(x,v,t) = N e^{-\frac{\beta m}{2}(v - v_0(x,t))^2} \rho(x,t) \tag{A.5}$$

and expand for small v_0. Keeping only the first order terms

$$p(x,v,t) \approx N e^{-\frac{\beta m}{2} v^2} \rho(x,t)(1 + v\beta m v_0(x,t))$$

and integrating we have

$$\rho(x,t) \approx N\rho(x,t) \int_{-\infty}^{+\infty} e^{-\frac{\beta m}{2} v^2}(1 + v\beta m v_0(x,t)) = \rho(x,t)$$

$$j(x,t) \approx N\rho(x,t) \int_{-\infty}^{+\infty} v e^{-\frac{\beta m}{2} v^2}(1 + v\beta m v_0(x,t)) = v_0(x,t)\rho(x,t)$$

where the first is simply a consistency check, and from the second one we get

$$p(x,v,t) \approx N e^{-\frac{\beta m}{2} v^2}(\rho(x,t) + v\beta m j(x,t)) \tag{A.6}$$

which is an expansion of $p(x,v,t)$ in orders of m in the over-damped limit. Now we can perform the last integral in A.4:

$$\int_{-\infty}^{+\infty} v^2 p(x,v,t)\,dv \approx N \int_{-\infty}^{+\infty} v^2 e^{-\frac{\beta m}{2}v^2}(\rho(x,t) + v\beta m j(x,t))\,dv = \frac{1}{\beta m}\rho(x,t)$$

A.4 becomes

$$\partial_t j(x,t) = \frac{-\partial_x \rho(x,t)}{\beta m} - \frac{\alpha}{m} j(x,t) - \frac{\partial_x U(x,t)}{m}$$

and keeping only leading terms as $m \to 0$:

$$j(x,t) \approx -\big(\frac{\partial_x \rho(x,t)}{\beta} + \rho(x,t)\partial_x U(x,t)\big)/\alpha$$

which in A.3 gives

$$\partial_t \rho(x,t) \approx -\partial_x\big(-\frac{\partial_x U(x,t)}{\alpha}\rho(x,t)\big) + \frac{1}{\beta\alpha}\partial^2_{xx}\rho(x,t) \tag{A.7}$$

a Fokker-Plank equation for $\rho(x,t)$ known as Smoluchowski's equation.

A.3 Mean first-passage time

We can know turn to our original problem: finding the average time a mesoscopic particle of mass m moving on the one-dimensional line under a potential $U(x)$ takes to escape from the segment $I = (x_1, x_2)$, starting from $x_0 \in I$. We include the cases where $x_1 \longrightarrow -\infty$ or $x_2 \longrightarrow +\infty$. Let $X(t)$ be the stochastic process describing the position of the particle at time t. The initial condition is $X(0) = x_0$. In the over damped limit $p(x,t|x_0,0)$ satisfies A.7. To simplify let us define $V(x) = U(x)/\alpha$ and $D = k_B T/m\gamma = 1/\beta\alpha$. Then we have

$$\begin{cases} \partial_t p(x,t|x_0,0) = -\partial_x(-\partial_x V(x) p(x,t|x_0,0)) + D\partial^2_{xx} p(x,t|x_0,0) = L_{FP} p(x,t|x_0,0) \\ p(x,0|x_0,0) = \delta(x - x_0) \end{cases} \tag{A.8}$$

It is useful to write L_{FP} in another way:

$$L_{FP} = D\partial_x e^{-\frac{V(x)}{D}} \partial_x e^{\frac{V(x)}{D}} \tag{A.9}$$

As we are interested in the distribution of the first passage time, we want to discard every realisation of $X(t)$ after it has exited I for the first time. In other words we want to "remove" every particle that gets to x_1 or x_2. This is achieved by restricting ourselves to I and considering its borders as absorbing boundaries:

$$p(x_1,t|x_0,0) = p(x_2,t|x_0,0) = 0$$

Let us now define $P_{x_0}(t)$ the probability that the process is still in I at time t. The subscript x_0 is to keep track of the starting position, and the starting time is fixed at $t = 0$ for simplicity. Then

$$P_{x_0}(t) = \int_{x_1}^{x_2} p(x,t|x_0,0)\,dx$$

Defining $w_{x_0}(t)$ the probability density of the first passage time, the probability of leaving I between t and $t + dt$ is

$$w_{x_0}(t)dt = -d(P_{x_0}(t)) = -\left(\int_{x_1}^{x_2} \partial_t p(x, t|x_0, 0)\, dx\right) dt$$

In principle we now have the distribution of the first passage time given a solution of the Fokker-Plank equation. Let us now see how we can derive the moments of the distribution without using an explicit solution for $p(x, t|x_0, 0)$.

$$\mathbb{E}[T] = \int_0^{+\infty} T w_{x_0}(T)\, dT = -\int_0^{+\infty} T \int_{x_1}^{x_2} \partial_t p(x, T|x_0, 0)\, dx\, dT =: \int_{x_1}^{x_2} p_1(x, x_0)\, dx$$

Integrating by parts we have

$$p_1(x, x_0) = -\int_0^{+\infty} T \partial_t p(x, T|x_0, 0)\, dT = \int_0^{+\infty} p(x, T|x_0, 0)\, dT$$

and applying L_{FP} to each side, using A.8, we get

$$L_{FP} p_1(x, x_0) = \int_0^{+\infty} \partial_t p(x, T|x_0, 0)\, dT = p(x, T|x_0, 0)|_{T=0}^{T=+\infty} = -\delta(x - x_0)$$

For the mean first passage time we have then

$$\begin{cases} \mathbb{E}[T] = \int_{x_1}^{x_2} p_1(x, x_0)\, dx \\ L_{FP} p_1(x, x_0) = -\delta(x - x_0) \end{cases} \tag{A.10}$$

A.4 Kramer's escape time

In this section we apply the method shown above to the problem of finding the mean time a particle takes to jump across a high-potential barrier. The shape of the potential is that in figure A.1: note that in the high barrier and low diffusion approximation we will consider, the details of the potential are not important, and only affect the result by small corrections.

Figure A.1: Potential for Kramer's escape problem

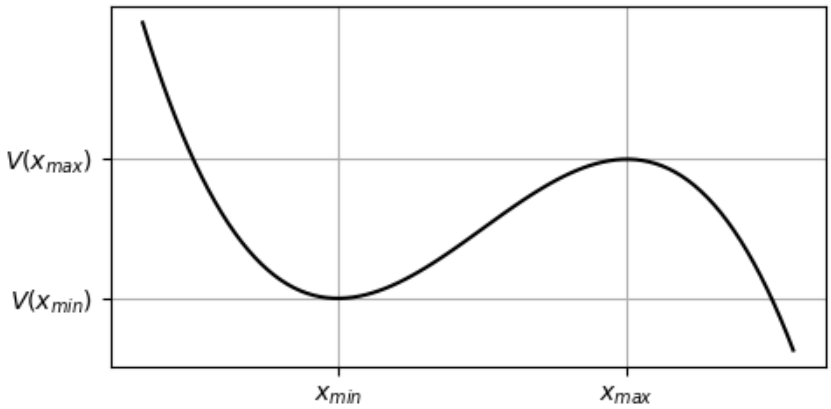

We have $I = (-\infty, x_{max})$ and restrict to the case of $x_0 = x_{min}$. In this specific case we have:

$$\mathbb{E}[T] = \int_{x_1}^{x_2} p_1(x, x_{min})\, dx$$
$$L_{FP} p_1(x, x_{min}) = -\delta(x - x_{min})$$

And the boundary condition for the absorbing wall at x_{max} implies

$$p_1(x_3, x_{min}) = 0 \,\forall\, x_3 > x_{max} \tag{A.11}$$

We wish to solve the following differential equation, obtained using A.9:

$$D\partial_x[e^{-\frac{V(x)}{D}} \partial_x (e^{\frac{V(x)}{D}} p_1(x, x_{min})] = -\delta(x - x_{min})$$

Integration between $-\infty$ and y gives:

$$De^{\frac{-V(y)}{D}} \partial_y (e^{\frac{V(y)}{D}} p_1(y, x_{min}) = -\int_{-\infty}^{y} \delta(x - x_{min})\, dx = -\theta(y - x_{min})$$

where $\theta(x)$ is the Heavside function. Integration between x and $x_3 > x_{max}$ now gives, using A.11:

$$-e^{\frac{V(x)}{D}} p_1(x, x_{min}) = -\int_{x}^{x_3} \frac{e^{\frac{V(y)}{D}}}{D} \theta(y - x_{min})\, dy$$

Then

$$\mathbb{E}[T] = \int_{-\infty}^{x_{max}} \frac{e^{\frac{-V(x)}{D}}}{D} \int_{x}^{x_3} e^{\frac{V(y)}{D}} \theta(y - x_{min})\, dy\, dx$$

The integral can be in principle performed once the explicit form of the potential is known. It is more interesting however to derive a result that is independent of such form and only depends on the fact that x_{min} is a point of minimum and x_{max} of maximum for $V(x)$. Then under the condition that the barrier is high ($\Delta V/D \gg 1$) we can expand $V(x)$ and extend the integrals over the whole line:

$$\int_{x}^{x_3} e^{\frac{V(y)}{D}} \theta(y - x_{min})\, dy \approx e^{\frac{V(x_{max})}{D}} \int_{-\infty}^{+\infty} e^{\frac{-|\partial_{xx}^2 V(x_{max})|(x - x_{max})}{2D}}\, dy = \frac{\sqrt{2D\pi} e^{\frac{V(x_{max})}{D}}}{\sqrt{|\partial_{xx}^2 V(x_{max})|}}$$
$$\int_{-\infty}^{x_{max}} e^{-\frac{V(x)}{D}}\, dx \approx e^{-\frac{V(x_{min})}{D}} \int_{-\infty}^{+\infty} e^{\frac{-\partial_{xx}^2 V(x_{min})(x - x_{min})}{2D}}\, dy = \frac{\sqrt{2D\pi} e^{-\frac{V(x_{min})}{D}}}{\sqrt{\partial_{xx}^2 V(x_{min})}}$$

Then

$$\mathbb{E}[T] \approx 2\pi \frac{e^{\frac{V(x_{max}) - V(x_{min})}{D}}}{\sqrt{\partial_{xx}^2 V(x_{min}) |\partial_{xx}^2 V(x_{max})|}} = \frac{2\pi k_B T}{D} \frac{e^{\frac{U(x_{max}) - U(x_{min})}{k_B T}}}{\sqrt{\partial_{xx}^2 U(x_{min}) |\partial_{xx}^2 U(x_{max})|}} =: \tau_0 e^{\beta \Delta U}$$